MSDE

PAPER

View Article Online
View Journal | View Issue

Cite this: *Mol. Syst. Des. Eng.*, 2025, **10**, 176

Investigating the design of macromolecular-based inks for two-photon 3D laser printing†

Samantha O. Catt, Clara Vazquez-Martel and Eva Blasco *

Received 26th September 2024,
Accepted 9th December 2024

DOI: 10.1039/d4me00160e

rsc.li/molecular-engineering

Two-photon 3D laser printing (2PLP) is one of the most versatile methods for additive manufacturing of micro- to nano-scale objects with arbitrary geometries and fine features. With advancing technological capability and accessibility, the demand for new and versatile inks is increasing, with a trend toward printing functional or responsive structures. One approach for ink design is the use of a macromolecular ink consisting of a 'pre-polymer' functionalized with photocrosslinkable groups to enable printability. However, so far the synthesis of pre-polymer inks for 2PLP often relies on an arbitrary choice rather than systematic design. Additionally, current structure–property relationship studies are limited to commercial or small molecule-based inks. Herein, three macromolecular inks with varied compositions, molecular weights, and glass transition temperatures are synthesized and formulated into inks for 2PLP. 3D microstructures are fabricated and characterized in-depth with scanning electron microscopy as well as infrared spectroscopy and nanoindentation to enable the determination of structure–processability–property relationships. Overall, it is clearly demonstrated that the macromolecular design plays a role in the printability and mechanical properties of the obtained materials.

Design, System, Application

Using controlled radical polymerisation methods, macromolecular-based inks that are suitable for two-photon 3D laser printing are designed. These macromolecules have varied compositions and chemical properties such as molecular weight, glass transition temperature, and comonomer compositions. Three monomers were chosen: butyl acrylate, methyl acrylate, and isobornyl acrylate, and copolymerized with the hydroxy group containing monomer 2-hydroxyethyl acrylate to give three low molecular weight and well defined macromolecules with differing properties. To introduce photocrosslinkable capability for two-photon 3D laser printing, the hydroxy groups were functionalized with acrylate moieties, allowing printable inks to be formulated from each macromolecule. The resultant structures were characterized and compared to determine their optimal printing parameters, the degree of conversion of the acrylate groups, and mechanical properties. Overall, we have shown that the molecular design affects the printability and the properties of the obtained material, *e.g.* reduced modulus. In addition, this precise molecular design allows structure–property relationships to be drawn for a deeper understanding of the effect of macromolecular properties on printing toward controlled and tailorable functional materials for their application in 3D printing.

1. Introduction

Two-photon 3D laser printing (2PLP), also referred to as direct laser writing (DLW), is a light-based additive manufacturing method allowing the fabrication of arbitrary 3D architectures in the micro- to nanoscale with high resolution. It relies on a photoreactive liquid (ink) that forms a solid material upon polymerization through two photon absorption processes. Among all of the materials utilized in 3D printing, polymer-based inks are one of the most promising printable materials due to their excellent versatility and adaptability. When focusing on light-triggered 3D printing, there exists a number of either commercially available or commonly used monomers employed in inks, of which acrylate-based crosslinking mechanisms are the most readily available and commonly used. Advances in technology and available set-ups for 2PLP in recent years has allowed for increasing material complexity, with a trend toward inks that allow for printing of functional and responsive structures.[1–3]

The inks used in 2PLP often include low molecular weight di-functional acrylates (*e.g.* ethylene glycol diacrylate) or tri- and tetra-acrylate derivatives, which can be crosslinked to create a stable polymeric network during the printing process. Another less employed strategy consists of the use of functional

Institute for Molecular Systems Engineering and Advanced Materials (IMSEAM), Heidelberg University, 69120 Heidelberg, Germany.
E-mail: eva.blasco@uni-heidelberg.de

† Electronic supplementary information (ESI) available. See DOI: https://doi.org/10.1039/d4me00160e

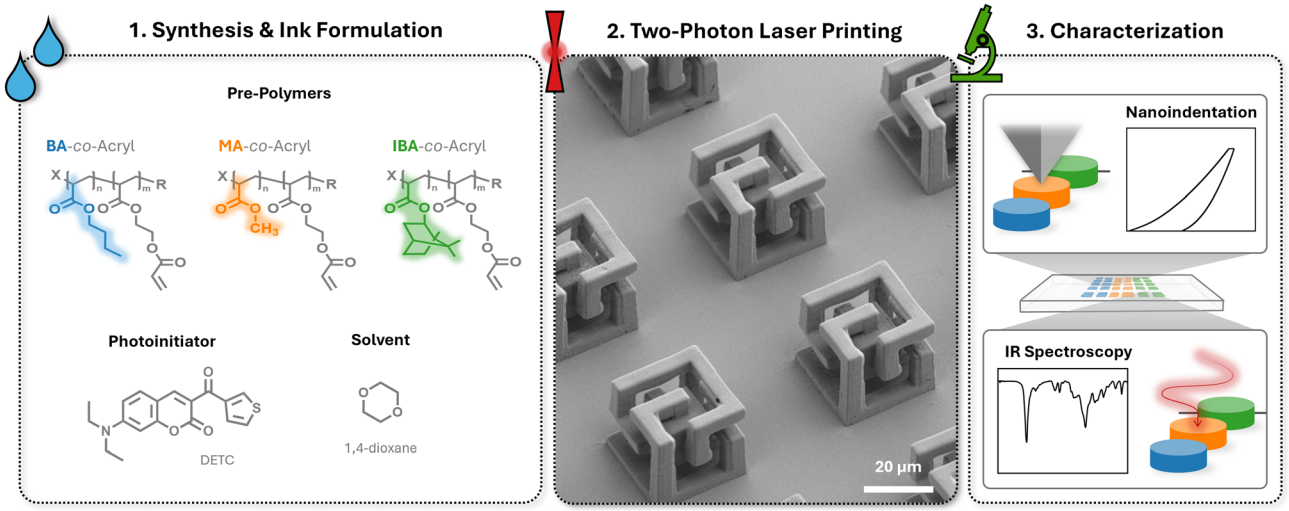

Scheme 1 Overall approach used to determine the structure–property relationships between three polymer inks BA-*co*-Acryl, MA-*co*-Acryl, and IBA-*co*-Acryl through 1) rational design of copolymer materials for ink formulation, 2) determination of optimum parameters using 2PLP and 3D printing microstructures, and 3) characterization through infrared spectroscopy and nanoindentation to determine chemical and mechanical properties, respectively.

photoreactive 'pre-polymers' as inks. This pre-polymer usually contains crosslinkable groups, which are introduced in a post-functionalization reaction, acting as reactive moieties during the printing process. For example, methacrylated biopolymers such as GelMA have been used extensively for printing applications.[4–6] Additionally, side-chain functionalized polymethacrylates were introduced by our group in the last years.[7,8] The advantage of this 'pre-polymer approach' is the incorporation of a larger amount of photocrosslinking and/or functional units per macromolecule with relatively low synthetic effort. With this strategy, when designing the material, initial composition such as the backbone, comonomer, and molecular weight, are often chosen arbitrarily or based on the existing literature. However, we propose that the macromolecular design can have drastic effects on the printability of the ink, as well as the resulting material properties of the printed structures.

Recent studies have made efforts to determine the influence of printing parameters in inks for 2PLP, for example the influence of laser power and scan speed, as well as the effects of photoinitiator choice on printability and resultant properties.[9–24] However, all of the current studies are limited to either inks based on commercial monomers (*e.g.* PETA, PEGDA[9,10,13,15,16,19,20]) or commercial inks (*e.g.* IP-DIP,[14,17,18,22,23] IP-S,[22] IP-L,[12] IP-PDMS[23] (Nanoscribe GmbH), SZ2080,[21] Sartomer 415 and Genomer 1330[11]) resulting in a lack of discernible correlation between the (macro)molecular composition of an ink with the resultant printing performance and structural properties. Recently, our group investigated the effect of molecular architecture on 2PLP through the intentional engineering of oligomer inks with sequence-controlled backbone compositions.[25] A clear correlation between the monomer sequence and the printability as well as the chemical and mechanical properties of resultant structures was observed. Despite clear indications that structure–property relationships exist, the effect of factors such as comonomer composition, glass transition temperature (T_g), *etc.* on printability, processability, and resultant material characteristics of 2PLP structures has not yet been studied in detail.

Herein, we present for the first time a strategy for the rational design of macromolecular inks for the study of structure–processability–property relationships of three polymers, in particular, comparing the influence of differing molecular composition by varying comonomers (Scheme 1). The three macromolecules are each comprised of two monomers: one comonomer containing the acrylate moiety as a sidechain to enable photocrosslinking, and a second comonomer that differs for each, either methyl (MA-*co*-Acryl), butyl (BA-*co*-Acryl) or isobornyl (IBA-*co*-Acryl) acrylate to test the influence of molecular structure differences and resulting properties, *i.e.* T_g, in the final material. Each polymer is formulated into an ink for 2PLP through the addition of a suitable photoinitiator and solvent and their printing performance using 2PLP is investigated. The resulting printed material is also characterized in terms of the degree of acrylate conversion through Fourier transform infrared (FTIR) spectroscopy, and the mechanical properties using nanoindentation. Together, the synthetic design, printing, and characterization gives insight into the structure–property relationships of macromolecules for 2PLP toward the systematic development of inks with well understood and tailorable properties.

2. Results and discussion

2.1 Design and synthesis of macromolecular-based inks

Reversible addition fragmentation transfer (RAFT) radical polymerization was used to synthesize copolymers for 2PLP (Fig. 1a). Reaction conditions were optimized in order to keep

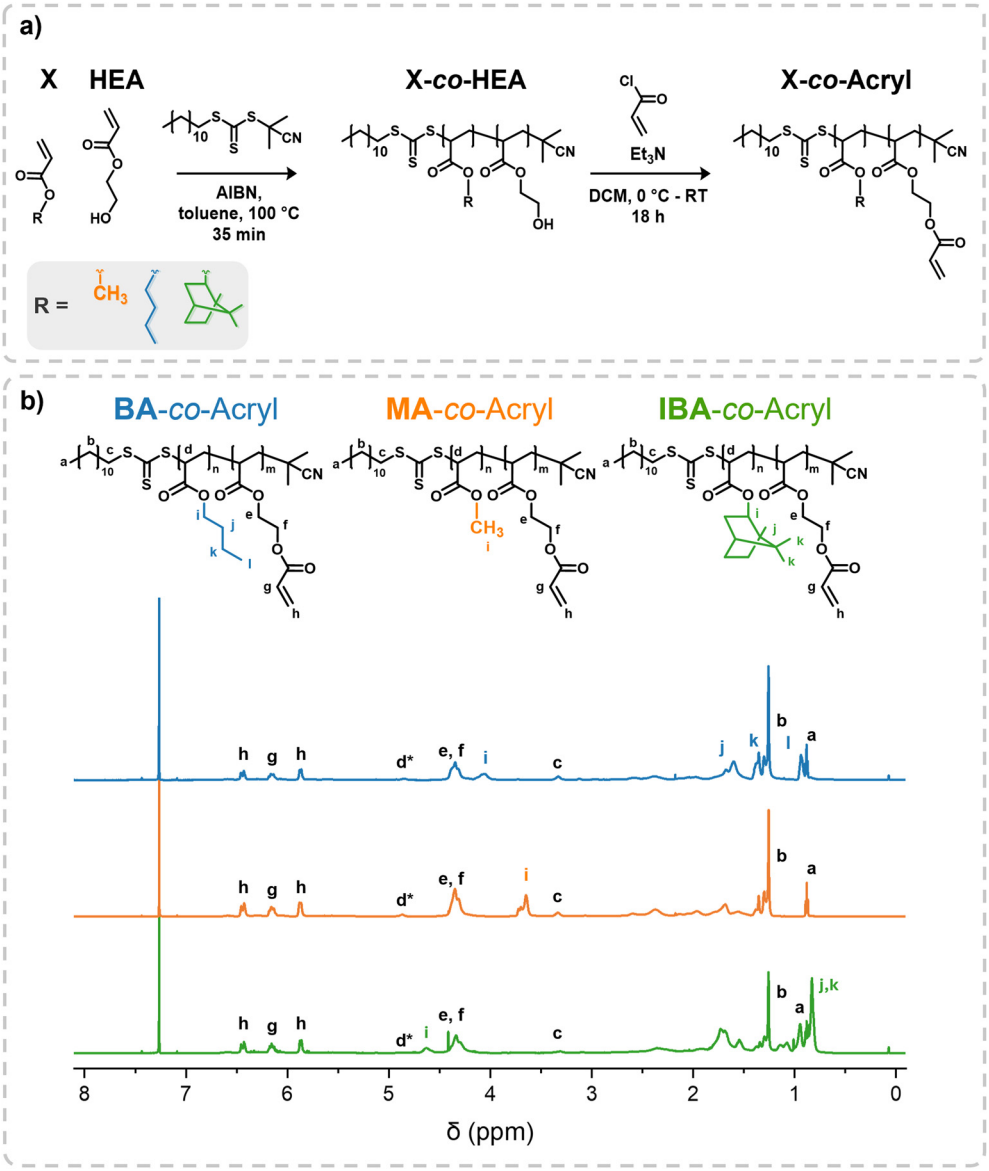

Fig. 1 a) Synthetic pathway for the preparation of each macromolecules using RAFT-controlled radical polymerization followed by functionalization with crosslinkable acrylate groups and b) ^{1}H-NMR spectra ($CDCl_3$, 600 MHz, 128 s, 295 K) of BA-*co*-Acryl (top, blue), MA-*co*-Acryl (middle, orange) and IBA-*co*-Acryl (bottom, green) polymers after post functionalization, where d* represents the protons of the monomer directly adjacent to the S of the chain transfer agent.

the resultant polymers at low molecular weight, and to decrease T_g and viscosity, for example reducing the required solvent concentration. Each macromolecule is composed of the monomer 2-hydroxyethyl acrylate (HEA) as well as a comonomer of either butyl acrylate, methyl acrylate, or isobornyl acrylate (further referred to as X) giving polymers of the conformation X-*co*-HEA.

These macromolecules (X-*co*-HEA) were characterized by ^{1}H nuclear magnetic resonance (NMR) spectroscopy (Fig. S1, ESI†) to determine their composition, size-exclusion chromatography (SEC) for molecular weight and dispersity ($Đ$), and differential scanning calorimetry (DSC) to determine glass transition temperature (T_g) (Fig. S2, ESI†). The hydroxy group of HEA was then used as a functional handle to introduce the reactive acrylate group, giving the conformation X-*co*-Acryl. The successful functionalization was confirmed by ^{1}H-NMR spectroscopy, where characteristic signals from the acrylate C=C double bond protons (Fig. 1b, $H_{g,\ h}$) appear between 5.8–6.5 ppm, as well as a downfield shift of the ethylene protons of HEA (H_f). After functionalization, repeat units of each monomer were determined through end group analysis using the protons adjacent to the S of the chain transfer agent (CTA) end group (H_c) at 3.3 ppm as reference. Conversion of the hydroxy of HEA was determined to be close to 100%, as evidenced in ^{1}H NMR spectra, with the downfield shift of the ethylene protons at 3.8 ppm (Fig. S1, ESI†).

The butyl (BA) sidechain copolymer has the lowest Mw (1500 g mol^{-1}) and lowest T_g (−44 °C) as well as the fewest

Table 1 Chemical and physical properties of polymers with varied co-monomer composition determined before or after post functionalization with acrylate

Co-monomer (X)	Mw_{GPC} (g mol^{-1})[a]	$Đ$[a]	T_g (°C)[a]	Acrylate (%)[b]	Acrylate units[b]	Comonomer (X) units[b]	Ratio Acryl : X[b]
BA	1500	1.05	−44	55.1	5.4	4.4	1 : 0.8
MA	1600	1.08	−42	56.3	6.3	4.9	1 : 0.8
IBA	2900	1.07	−5	54.7	8.1	6.7	1 : 0.8

[a] Unfunctionalized (X-*co*-HEA). [b] Functionalized (X-*co*-Acryl).

number of acrylate units (5.4). The methyl (MA) sidechain copolymer has a slightly higher Mw (1600 g mol^{-1}), T_g (−42 °C) and number of acrylate units (6.3). The isobornyl sidechain (IBA) copolymer has the highest Mw (2900 g mol^{-1}), T_g (−5 °C) and number of acrylate units (8.1). The ratio of acrylate repeat units to comonomer units is similar for all three polymers with approximately 55% and a ratio (Acryl : X) of 1 : 0.8. Additionally, all polymers have a dispersity below 1.1. Differences in T_g arise from the differing chemical composition, and the effect of increased photocrosslinkable groups is also investigated through the synthesis of a slightly larger polymer (IBA-*co*-Acryl). The results of the synthesis of the three polymers, with characterization before or after post functionalization with acrylate, are summarized in Table 1.

2.2 Ink formulation and two-photon 3D laser printing (2PLP)

A typical ink for 2PLP is composed of the crosslinkable monomer(s) or polymer(s) and a suitable photoinitiator. To improve the solubility of the photoinitiator or monomers/polymers, a solvent may be needed. In this work, to determine the relationship between the molecular structure, physical properties and printability, each polymer was formulated into an ink of similar composition. For this purpose, the only varied parameter was the macromolecule, whereas the concentration of photoinitiator and solvent remained constant. The optimized formulation for all inks comprised 66 wt% of polymer (IBA-*co*-Acryl, BA-*co*-Acryl, or MA-*co*-Acryl), 0.5 wt% 7-diethylamino-3-thenoylcoumarin (DETC) as photoinitiator, and the remainder of the ink is composed of 1,4-dioxane as the solvent to improve solubility and viscosity.

The printability of each ink was examined by printing buckyball microstructures 60 μm in diameter over a laser power range of 15–40 mW with 2.5 mW increments, and a scan speed window of 10, 15, or 20 mm s^{-1}. Structures were imaged using scanning electron microscopy (SEM). This range, termed here as the window of printability, was determined as the range whereby the buckyball structures were standing with no visible defects such as partial collapse, closed pores, or explosion effects (Fig. 2). Below this threshold at lower laser powers the structures are insufficiently formed. Either the structure is completely unformed and removed during development, or residual material remains but the structures collapse due to insufficient network formation. At higher laser powers, so-called microexplosions occur leading to uncontrolled polymerization.

From the structures characterized over the range of laser powers and scan speeds, it is apparent that the BA-*co*-Acryl ink has the smallest window of printability, followed by MA-

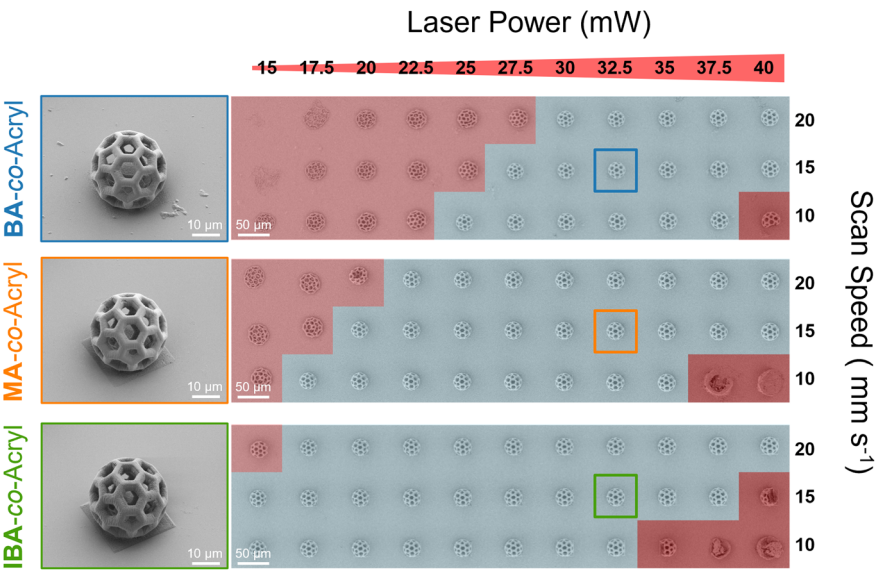

Fig. 2 SEM images of buckyballs printed with the three polymer inks with varied laser power (15–40 mW) and scan speed (10, 15, 20 mm s^{-1}) showing the determined printability range of each ink. The window of printability is determined as the laser power and scan speed parameters where the structures remained stable (blue), above and below this range under or overexposure occurred (red). Representative SEM images of structures printed with parameters within the printing window with the three inks BA-*co*-Acryl, MA-*co*-Acryl, and IBA-*co*-Acryl are highlighted.

co-Acryl. A comparison of single line printing to examine the thickness of each ink at the same laser power and scan speed parameters is included in Fig. S4, ESI.† The printable range for IBA-*co*-Acryl is larger, with a lower laser power required for stable structures, however more overexposure was observed at higher laser powers than for the two other polymers. Focusing on a scan speed of 15 mm s^{-1}, the window of printability for BA-*co*-Acryl is between 27.5–40 mW, while for MA-*co*-Acryl is it 20–40 mW. From the macromolecular properties determined for each of the polymers, BA and MA have similar T_g and Mw, however BA has slightly fewer acrylate units overall (5.4) compared to MA (6.3), potentially increasing the printability range. This is further supported by the larger printability range observed for IBA-*co*-Acryl, which has even more acrylate units (8.1). However, when considering the effect of comonomer, the IBA polymer additionally has a higher T_g and Mw, which may also increase the printability range.

2.3 In depth characterization of 3D printed microstructures

For a deeper insight into the relationship between macromolecular structure and printability, printed structures were also analyzed using FTIR spectroscopy and nanoindentation to determine the degree of acrylate conversion (DC) and reduced modulus (E_r), respectively, for a range of laser powers. For consistency, a scan speed of 15 mm s^{-1} was used for 2PLP of all structures. Upon 3D printing, the acrylate double bonds are consumed as they react through two-photon absorption-initiated free-radical polymerization. By comparing the IR spectra of the printed structures (40 × 40 × 10 μm^3 cubes) with the IR spectrum of the unprinted material, an overall degree of acrylate conversion, *i.e.* the percentage of acrylate consumed during printing, can be determined (Fig. S3, ESI†). It was observed for all inks that as the laser power increased, so too did the conversion degree (Fig. 3a), as reported previously in the literature.[9,10,20] As the printability range varies for each ink, the lower threshold for measurement of DC and E_r also varies, as seen by the gray dashed lines (Fig. 3a and b). Below this threshold laser power, the structures were unmeasurable. Overall, the degree of acrylate conversion for all three inks was similar. For IBA-*co*-Acryl the range of conversion was 51–68% over the measurable laser power window of 15–40 mW. The range for MA-*co*-Acryl was determined to be 52–68% for 22.5–40 mW. For BA-*co*-Acryl it was 45–69% for 25–40 mW. This suggests that above a minimum DC threshold, in all three cases approximately 45–50%, stable structures will be formed, which can be measured. Importantly, the laser power required to achieve this threshold is dependent on the ink used, where IBA required the lowest laser power to reach this conversion threshold, followed by MA-*co*-Acryl, and BA-*co*-Acryl, which required the highest laser power. The printability study presented in Fig. 2 supports this, where the lower range for printable structures was 15, 20, and 27.5 mW for IBA, MA, and BA, respectively.

Nanoindentation was used to measure the mechanical properties of each ink. For this, micropillars were printed with a diameter of 60 μm and a height of 15 μm. A similar trend was observed when measuring nanoindentation as for FTIR spectroscopy, where the lower laser power limit for characterizable structures was 17.5, 20, and 25 mW for IBA-*co*-Acryl, MA-*co*-Acryl, and BA-*co*-Acryl, respectively. An overview of the lower threshold values can be seen in Fig. S5, ESI.† Above the threshold laser power, the pillars appear similar to the desired geometry, whereas below this threshold some deviation is observed, for example as shown for BA-*co*-Acryl in Fig. 3b. The results show that overall, for all laser powers, IBA-*co*-Acryl generally has the highest E_r, reaching 2.6 GPa at 40 mW. Interestingly, for IBA-*co*-Acryl the trend of increasing arylate conversion does not correlate with the E_r measured, where the modulus remains relatively constant over the entire range of measured laser powers. For the MA-*co*-Acryl structures, the E_r increases from a minimum of 1.6 GPa at 20 mW laser power to 2.8 GPa at 40 mW, reaching a slightly higher E_r as IBA-*co*-Acryl above 35 mW. On the other hand, BA-*co*-Acryl has a lower E_r over each of the measured laser powers, from 1.1–1.5 GPa for 25–40 mW, respectively.

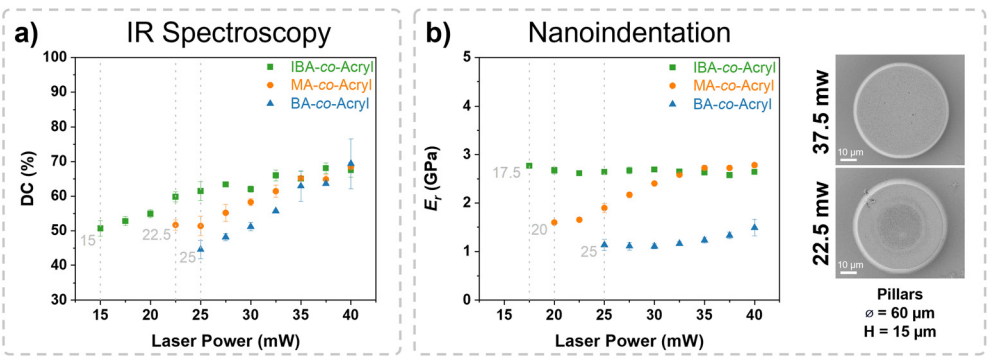

Fig. 3 a) Degree of acrylate conversion (DC) measured through IR spectroscopy of microstructures printed with varied laser powers and b) reduced modulus (E_r) measured using nanoindentation for the three inks IBA-*co*-Acryl (green), MA-*co*-Acryl (orange), and BA-*co*-Acryl (blue) and SEM images of example structures used for nanoindentation measurements printed with at lower and higher laser power using BA-*co*-Acryl. Error bars represent standard deviation where n = 3 for all measurements, where reasonably possible.

Despite the increase in DC from 44.5 to 69.4% over the laser power range, the increase in E_r is not as significant when compared, for example, to the increase observed for MA-*co*-Acryl of 1.2 GPa over a similar DC range (51.7–68.5%).

These trends may potentially be attributed to the macromolecular architecture of the polymer and the topology of the network within the printed structure. For example, as seen previously, dangling chains such as butyl groups within the network can give an overall softening effect on the mechanical properties despite a similar degree of acrylate conversion.[25,26] This may be apparent when comparing MA-*co*-Acryl and BA-*co*-Acryl inks, which have a similar T_g and molecular weight, as well as similar number of acrylate units, as the effect of the comonomer becomes more significant. Additionally, despite the similarities to MA-*co*-Acryl, a higher laser power is required to reach higher DC values for BA-*co*-Acryl, suggesting an influence of the comonomer of the macromolecule during the crosslinking process. This is consistent with the idea that network formation is dependent on the macromolecular structure as well as the chemical and physical processes occurring during photopolymerization.[27] Considering the IBA-*co*-Acryl ink, E_r and DC are higher at all laser powers and a lower laser power is required to reach the conversion threshold for printing stable structures. Where for BA-*co*-Acryl the butyl chain acts as a softener to reduce the mechanical properties, here the IBA groups as well as the larger Mw increase the T_g, which may contribute to the increased printability range and higher E_r of IBA-*co*-Acryl materials.

To demonstrate the printing performance of the three inks in terms of geometrical complexity, multiple 3D microstructures were printed at a constant laser power and scan speed (32.5 mW, and 15 mm s^{-1}, respectively), for example, the fullerene buckyball with a diameter of 30 μm, a model of the Sydney Opera House on a platform with a diameter of 60 μm and a height of 20 μm, or a 15 μm^3 geometrical cubic structure (Fig. 4). It is clear that it is possible to print high resolution 3D structures with overhangs and fine features using all three investigated inks.

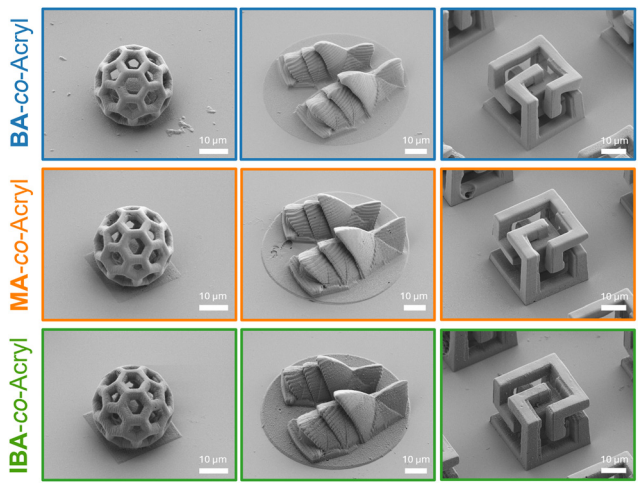

Fig. 4 SEM images of 3D structures printed with high resolution and fine features printed using all three inks at the same printing parameters (32.5 mW and 15 mm s^{-1}).

3. Summary and outlook

For the first time, structure–property relationships of rationally designed macromolecular inks are investigated for 2PLP. We determine the influence of varied monomer and molecular composition on the printability and resultant properties of structures printed with three different inks. We have identified notable effects depending on the macromolecular composition of the inks in terms of printability, as well as the degree of acrylate conversion and the resultant mechanical properties of the three polymers. For the BA-*co*-Acryl ink, the lowest E_r was observed, with only a slight increase observed from lowest to highest laser power. Additionally, despite all inks forming stable printed structures at similar DC, the laser power required to reach that DC threshold differed. For example, higher laser power was required to reach the minimum threshold of acrylate conversion to print stable structures for BA-*co*-Acryl. For MA-*co*-Acryl, a higher increase in E_r was observed over the laser power range, and overall the material was stiffer than BA-*co*-Acryl, but softer than IBA-*co*-Acryl. The IBA-*co*-Acryl ink had the highest E_r, as well as the largest window of printability, at all laser powers, appearing to be the most versatile of the three inks that were investigated. Thus, it is clear that the comonomer choice as well as molecular design significantly influence the printing behavior and resultant properties of the printed material, and should be considered when designing inks for specific applications. We show that through careful consideration, it is possible to created tailored material properties in 3D printed microstructures. This study represents a crucial advancement in establishing an initial framework for understanding the correlations between ink design and resultant material properties.

4. Experimental

Chemicals and materials

Chemicals and solvents were supplied from either Sigma-Aldrich or Fisher Scientific unless otherwise mentioned. All materials were used as received without further purification unless indicated. Acrylate monomers were filtered through basic alumina prior to use.

Synthesis and characterization

Full synthetic details are provided in the ESI.† Characterization was performed with ^{1}H-nuclear magnetic resonance (NMR) spectroscopy (Bruker Avance III 600 or Bruker Avance III 300, 128 scans, relaxation delay 0.1 s or 1 s, respectively, 295 K).

Size Exclusion Chromatography (SEC)

SEC measurements were performed on a Shimadzu Nexera LC-40 system (with LC-40D pump, autosampler SIL-40C, DGU-403 (degasser), CBM-40 (controlling unit), column oven CTO-40C,

UV-detector SPD40, and RI-detector RID-20A). The system was equipped with 4 analytical GPC-columns (PSS): 1 × SDV precolumn 3 μm 8 × 50 mm, 2 × SDV column 3 μm 1000 Å 8 × 300 mm, 1 × SDV column 3 μm 10 × 10^4 Å 8 × 300 mm. The measurements were performed in tetrahydrofuran at a flow rate of 1 mL min^{-1} at a temperature of 40 °C. Chromatograms were analyzed using LabSolutions (Shimadzu) software. Calibration was performed against different polymethylmethacrylate standards (800–2 200 000 Da, PSS).

Ink preparation

Under yellow light conditions, a stock solution of DETC in 1,4-dioxane was added to the dried monomer in a 2 mL Eppendorf tube to give a final composition of 0.5 wt% DETC, 66.6 wt% monomer in dioxane. The ink was centrifuged for 5 min at 150 rpm, then left shaking overnight to ensure homogeneity. The ink was used within one day of preparation.

Silanization procedure

Glass coverslips (Marienfeld, 170 ± 5 μm) were washed with isopropanol and acetone and dried using pressurized N_2. Subsequently, the surface was activated for one minute by plasma treatment. The coverslips were immersed in a 4 × 10^{-3} M solution of 3-(trimethoxysilyl)propyl acrylate in toluene for 1.5 h. After washing twice in toluene and once in acetone then drying under N_2 flow, the acrylate-functionalized glass slides were stored under yellow light conditions.

Scanning electron microscopy

Scanning electron microscopy (SEM) was performed with a Zeiss Supra 55VP (Carl Zeiss AG) at 3 kV in secondary electron mode. Prior to imaging, the structures were sputter-coated with a 12 nm layer of Pd:Pt.

Differential scanning calorimetry

DSC measurements were conducted with a Discovery DSC 250 of TA Instruments on polymer samples with 3–4 mg weight and a heating and cooling rate of 10 °C min^{-1}. Measurements were conducted on non-acrylated polymers prior to post functionalization.

Two-photon laser printing

2PLP was performed employing a Photonic Professional GT2 (Nanoscribe GmbH) system. Microfabrication of all structures was performed in oil immersion mode with a femtosecond laser (λ = 780 nm) focused through a 63× oil objective lens (NA = 1.4; Zeiss). Employing Describe software (Nanoscribe), GWL files were generated from STL files of desired geometries and executed by the printer for 3D structure fabrication. Slicing was set to 300 nm and hatching to 200 nm for all microgeometries. Printing was performed with a scan speed of 15 mm s^{-1} and laser power in the range of 15 to 40 mW unless otherwise stated. To ensure stability of the samples, the ink was loaded into a PDMS mold and sealed with a coverslip during printing. Fabricated structures on glass substrates were developed for 8 min in acetone, followed by drying in air. The maximum output of the instrument is 50 mW.

Fourier-Transform Infrared (FT-IR) spectroscopy

Blocks (40 × 40 × 10 μm^3) were fabricated using 2PLP. FT-IR spectra were collected with an FT-IR microscope (LUMOS-II, Bruker) in attenuated total reflectance (ATR) configuration, 64 scans, with a liquid N_2 cooled detector. For all data points, n = 3 samples were printed and measured for each scan speed and laser power parameter. The mean for the three spectra for each printed structure was calculated, and the average of the three structures was used for standard deviation calculations. Before averaging, each spectrum was baseline corrected and normalized against the peak of ν (C═O) (1725 cm^{-1}). The ratio of the area of ν (C═O) (1850–1655 cm^{-1}) and ν (C═C) (830–780 cm^{-1}) was determined and compared with the functionalized polymer before printing to determine the overall acrylate conversion as per eqn (S1). The functionalized polymer (ink) was measured on a JASCO FT/IR-4600 FT-IR spectrometer (128 scans).

$$\mathrm{DC}\ \% = 1 - \frac{(A_{C=C}/A_{O\text{-}C=O})}{(A^{ink}_{C=C}/A^{ink}_{O\text{-}C=O})} \times 100 \quad \text{(S1)}$$

Nanoindentation

Micropillars (z-height = 15 μm, Ø = 60 μm) were fabricated using 2PLP. For the measurement of the mechanical properties, nanoindentation measurements were performed with a Bruker Hysitron TI 980. For all measurements, a diamond Berkovich tip was used with automatic drift control. As test protocol, a standard trapezoid loading function was applied. For all samples, where possible, n = 3 measurements were carried out on random positions and a mean value with standard deviation was calculated from the obtained results. The reduced modulus (elastic modulus) was calculated according to published work.[28]

Data availability

Data for this article, including raw data of the characterization of the materials and images, are available at the HeiData repository (**https://doi.org/10.11588/data/ESNDA6**).

Conflicts of interest

There are no conflicts to declare.

Acknowledgements

The authors acknowledge the funding from the Deutsche Forschungsgemeinschaft (DFG, German Research Foundation)

via the Excellence Cluster "3D Matter Made to Order" (EXC-2082/1-390761711), the Carl Zeiss Foundation through the Carl-Zeiss-Foundation-Focus@HEiKA, and the Baden Württemberg Ministry. E. B. thanks the Federal Ministry of Education and Research (BMBF) and the Ministry of Science Baden-Württemberg within the framework of the Excellence Strategy of the Federal and State Governments of Germany. C. V. M. acknowledges the Fonds der Chemischen Industrie for the financial support (Kekulé Fellowship). The authors thank P. Mainik for performing DSC measurements, and B. Weidinger for many fruitful discussions. In addition, R. Schröder, I. Wagner and R. Curticean are thanked for the access and training at the electron microscopy facilities.

References

1 P. Mainik, C. A. Spiegel and E. Blasco, *Adv. Mater.*, 2024, **36**, 2310100.
2 C. L. Lay, C. S. L. Koh, Y. H. Lee, G. C. Phan-Quang, H. Y. F. Sim, S. X. Leong, X. Han, I. Y. Phang and X. Y. Ling, *ACS Appl. Mater. Interfaces*, 2020, **12**, 10061–10079.
3 S. O'Halloran, A. Pandit, A. Heise and A. Kellett, *Adv. Sci.*, 2023, **10**, 2204072.
4 A. I. Van Den Bulcke, B. Bogdanov, N. De Rooze, E. H. Schacht, M. Cornelissen and H. Berghmans, *Biomacromolecules*, 2000, **1**, 31–38.
5 A. Ovsianikov, A. Deiwick, S. van Vlierberghe, M. Pflaum, M. Wilhelmi, P. Dubruel and B. Chichkov, *Materials*, 2010, **4**, 288–299.
6 R. Levato, K. S. Lim, W. Li, A. U. Asua, L. B. Peña, M. Wang, M. Falandt, P. N. Bernal, D. Gawlitta, Y. S. Zhang, T. B. F. Woodfield and J. Malda, *Mater. Today Bio*, 2021, **12**, 100162.
7 P. Müller, R. Müller, L. Hammer, C. Barner-Kowollik, M. Wegener and E. Blasco, *Chem. Mater.*, 2019, **31**, 1966–1972.
8 B. Weidinger, G. Yang, N. Von Coelln, H. Nirschl, I. Wacker, P. Tegeder, R. R. Schröder and E. Blasco, *Adv. Sci.*, 2023, **10**, 2302756.
9 T. Baldacchini, M. Zimmerley, C.-H. Kuo, E. O. Potma and R. Zadoyan, *J. Phys. Chem. B*, 2009, **113**, 12663–12668.
10 K. Cicha, Z. Li, K. Stadlmann, A. Ovsianikov, R. Markut-Kohl, R. Liska and J. Stampfl, *J. Appl. Phys.*, 2011, **110**, 064911.
11 K. Cicha, T. Koch, J. Torgersen, Z. Li, R. Liska and J. Stampfl, *J. Appl. Phys.*, 2012, **112**, 094906.
12 L. J. Jiang, Y. S. Zhou, W. Xiong, Y. Gao, X. Huang and L. Jiang, *Opt. Lett.*, 2014, **39**, 3034–3037.
13 L. Jiang, W. Xiong, Y. Zhou, Y. Liu, X. Huang, D. Li, T. Baldacchini, L. Jiang and Y. Lu, *Opt. Express*, 2016, **24**, 13687.
14 E. D. Lemma, F. Rizzi, T. Dattoma, B. Spagnolo, L. Sileo, A. Qualtieri, M. de Vittorio and F. Pisanello, *IEEE Trans. Nanotechnol.*, 2017, **16**, 23–31.
15 X. Gou, M. Zheng, Y. Zhao, X. Dong, F. Jin, J. Xing and X. Duan, *Appl. Surf. Sci.*, 2017, **416**, 273–280.
16 T. Zandrini, N. Liaros, L. J. Jiang, Y. F. Lu, J. T. Fourkas, R. Osellame and T. Baldacchini, *Opt. Mater. Express*, 2019, **9**, 2601.
17 J. Bauer, A. G. Izard, Y. Zhang, T. Baldacchini and L. Valdevit, *Adv. Mater. Technol.*, 2019, **4**, 1900146.
18 I. S. Ladner, M. A. Cullinan and S. K. Saha, *RSC Adv.*, 2019, **9**, 28808–28813.
19 M. Belqat, X. Wu, L. P. C. Gomez, J.-P. Malval, S. Dominici, B. Leuschel, A. Spangenberg and K. Mougin, *Addit. Manuf.*, 2021, **47**, 102232.
20 Q. Hu, G. A. Rance, G. F. Trindade, D. Pervan, L. Jiang, A. Foerster, L. Turyanska, C. Tuck, D. J. Irvine, R. Hague and R. D. Wildman, *Addit. Manuf.*, 2022, **51**, 102575.
21 L. Pertoldi, V. Zega, C. Comi and R. Osellame, *J. Appl. Phys.*, 2020, **128**, 175102.
22 M. Diamantopoulou, N. Karathanasopoulos and D. Mohr, *Addit. Manuf.*, 2021, **47**, 102266.
23 S. Schweiger, T. Schulze, S. Schlipf, P. Reinig and H. Schenk, *J. Opt. Microsyst.*, 2022, **2**, 033501.
24 P. F. J. Van Altena and A. Accardo, *Polymers*, 2023, **15**, 1816.
25 S. O. Catt, M. Hackner, J. P. Spatz and E. Blasco, *Small*, 2023, **19**, 2300844.
26 E. A. Hoff, G. X. De Hoe, C. M. Mulvaney, M. A. Hillmyer and C. A. Alabi, *J. Am. Chem. Soc.*, 2020, **142**, 6729–6736.
27 P. Somers, A. Münchinger, S. Maruo, C. Moser, X. Xu and M. Wegener, *Nat. Rev. Phys.*, 2024, **6**, 99–113.
28 W. C. Oliver and G. M. Pharr, *J. Mater. Res.*, 1992, **7**, 1564–1583.